IEEE Access
Multidisciplinary | Rapid Review | Open Access Journal

Received August 23, 2019, accepted September 10, 2019, date of publication September 13, 2019,
date of current version September 26, 2019.

Digital Object Identifier 10.1109/ACCESS.2019.2941466

On the Relationship Between the Electromagnetic Burst and Inductive Sensor Measurement of a Pulsed Plasma Accelerator

LUIS ORELLANA[1], JORGE ARDILA-REY[1], GONZALO AVARIA[2,3], MARCOS A. DÍAZ[4], CRISTIAN PAVEZ[2,3], ROGER SCHURCH[1], (Member, IEEE), AND LEOPOLDO SOTO[2,3]

[1]Department of Electrical Engineering, Federico Santa María Technical University, Santiago 8940000, Chile
[2]Departamento de Ciencias Nucleares, Comisión Chilena de Energía Nuclear, Casilla 188-D, Chile
[3]Departamento de Ciencias Físicas, Facultad de Ciencias Exactas, Universidad Andres Bello, Santiago 8370035, Chile
[4]Department of Electrical Engineering, Faculty of Physical and Mathematical Sciences, University of Chile, Santiago 8370451, Chile

Corresponding author: Luis Orellana (luis.orellanag@alumnos.usm.cl)

This work was supported in part by Fondecyt Iniciación under Grant 11160115, in part by Federico Santa María Technical University Grant Project PI_m_19_01, and in part by Dirección de Postgrados y Programas of Federico Santa María Technical University under PIIC Grant.

ABSTRACT A remote and non-invasive diagnostic of the plasma focus using antennas is presented in this work. The main motivation is the application of such diagnostic in a miniaturized plasma accelerator, based on the plasma focus architecture, as a cube satellite thruster. The evaluation of this proposal was carried out measuring a hundred of joules plasma focus operation simultaneously with the inductive measurement and antennas. Three different antennas tuned in the ultra high frequency range were tested: a monopole, Vivaldi and helical. The high frequency transients detected with the antennas were time correlated to the known inductive measurement features. The initial dielectric breakdown and later plasma pinch and subsequent disruption (i.e. the source of the propulsion) were identified to be the principal phenomena to be detected. Signal parameter correlations between the inductive sensor and the antennas showed that the pinch phenomena can be correlated with the antenna signals. Good correlation results were obtained with the monopole antenna when using peak value and signal energy parameter from the antenna transient. An improvement in the correlation results, for the helical and Vivaldi antennas, was obtained when calculating the frequency band energy. In this case, the Vivaldi antenna achieved the best results. The results of the monopole antenna make it an alternative remote sensor for plasma focus, but for the application of a miniaturized plasma focus as pulsed plasma thruster, the Vivaldi antenna is a more feasible design to replace the inductive diagnostic due to its compact design in comparison to the monopole.

INDEX TERMS Inductive sensor, pulsed plasma thruster, plasma focus, ultra high frequency antennas.

I. INTRODUCTION

The trend of standardized satellites (CubeSats) technology [1], in particular the nanosatellite class [2], has motivated ever-increasing interest in its developing technologies and applications such as measurements for space science, weather and climate, topics in astrophysics, planetary science, communications and remote sensing. Different institutions, companies and countries are either proposing or developing novel missions based on Cubesats (or a constellation of them) [3]–[7]. The CubeSats development needs to address the technological issues of precision attitude control and propulsion [8]. Different propulsion systems have been studied and developed [9], [10], being the pulsed plasma accelerator of the plasma focus type, an attractive alternative due to its scaling capabilities [11], [12] that allow the transition from high energy and size devices into smaller and compact ones. The possible adaptation of a dense plasma focus (DPF) for its application as pulsed plasma accelerator, i.e. a pulsed plasma thruster (PPT), motivates the present work. DPFs are devices where a magnetized and high temperature plasma is produced during a few to hundreds of nanoseconds by an electric discharge [13]. Those pulsed power devices are a type of Z-pinch [14] that corresponds to a magnetic confinement

The associate editor coordinating the review of this manuscript and approving it for publication was Giorgio Montisci.

This work is licensed under a Creative Commons Attribution 4.0 License. For more information, see http://creativecommons.org/licenses/by/4.0/

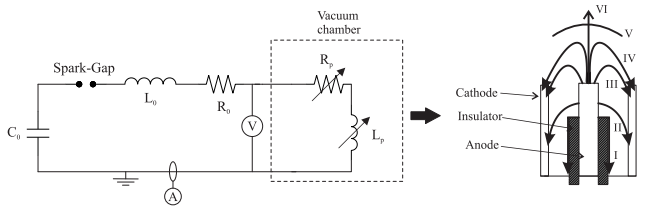

FIGURE 1. A general schematic and simplified external circuit of a plasma focus device. To the right the DPF stages are highlighted.

configuration. DPF can produce high intensity pulsed electromagnetic radiation, in a wide frequency spectrum from radio frequency to X rays, as well as charged and neutral particles. Some applications of these devices are: pulsed source of X rays [15] and neutrons [16]–[19], the production of plasma shocks and testing of fusion reactor wall materials [20], [21], as ion beam accelerator [22], pulsed irradiation for cancerous cells [23] and the intended application as a PPT, potentially for its use in CubeSat propulsion. The DPF architecture considered in this work is a capacitor based discharge [24], [25], specifically, the discharge of a capacitor bank into a coaxial electrode system inside a vacuum chamber and switched via spark-gap. The plasma dynamics of the DPF take place inside a vacuum chamber which is filled with a working gas at low pressure in the range of 1 mbar to 10 mbar. DPF, as an electric device, can be understood by a simple RLC underdamped circuit model [25], see Fig. 1. The driver of the circuit, i.e. the capacitor bank and its connection to the vacuum chamber electrodes, is modeled as an equivalent capacitance C_0 for the bank and equivalent losses R_0 and inherent, or stray, inductance L_0 of both the capacitor bank and connection leads. The plasma dynamics occurring inside the chamber have been modeled as a time-variant resistance R_p and inductance L_p [24]–[26].

As can be seen in Fig. 1, the discharge process can be explained in six stages [13], [25], [27]. In stage **I** the initial gas breakdown occurs and creates a plasma sheath on the surface of the insulator. Next, in stage **II**, the plasma sheath is axially accelerated towards the end of the electrodes due to its interaction with the magnetic field of the current on the anode. In stage **III**, the plasma sheath, on top of the anode, experiences a radial acceleration that compresses it because of the self induced Lorentz force (z-pinch). In stage **IV**, the plasma is compressed into a dense column and reaches a stagnation point, thus maximum compression is achieved that lasts around a few to hundreds of nanoseconds, depending on the device energy. This important stage of the discharge is called pinch [25]. Then, due to not being in equilibrium in the axial direction, plasma from the column escapes the confinement. This process is called pinch disruption and leads to the ejection of plasma shocks [20] in the axial direction, stage **V**. Finally, in stage **VI**, as the plasma shock advances, plasma jets are ejected from the anode [28]. The pinch developed by the discharge, stage **IV**, is the main feature of the DPF as a source of high energy radiation, neutrons and beams. The conditions for the emission of high energy electromagnetic radiation, such as X rays and particle beams, are achieved in the pinch stage [25]. Moreover, because of pinch disruption, the plasma shock and plasma jets are emitted. The initial speed of the plasma shock is in the order of $5 \cdot 10^5$ m/s [20] or greater, and the plasma jets speed is in the order of $4 \cdot 10^4$ m/s [28]. These are the principal phenomena to be used in a PPT.

DPF operation is typically diagnosed electrically using inductive sensors, in particular Rogowski coils, to measure the time derivative of the circuit current, and a voltage divider, to measure the time evolution of the voltage at the vacuum chamber electrodes [24], [25]. See Fig. 1: (A) the Rogowski coil and (V) the voltage divider. The inductive sensors are wrapped around the returning leads that connect the vacuum chamber to the capacitor bank, meanwhile the voltage divider is connected as close as possible to the anode [24], [25]. Both the Rogowski coil and voltage divider have limitations, specially with the bandwidth. An adequate bandwidth is required to detect the fast pinch stage. On one side, the Rogowski coil is a compromise between number of turns (its gain) and the resultant bandwidth. Even the proper location of the Rogowski coil with respect to the current path to be measured is paramount for its performance and calibration. On the other, fast voltage dividers with picosecond rise time had only be achieved with ion solution resistances [29]. Considering the intended nanosatellite application, both sensors are placed as close as possible to the DPF, so they impose a risk of failure due to disconnection or undesired electric contact. Also, a close connection of this kind is not recommended since the structure will be subjected to extreme movement and vibration stresses [30].

A remote sensor based on the measurement of the electromagnetic (EM) burst from a DPF, basically an antenna working as a receptor, is the diagnostic method evaluated in this work. Previously, radiofrequency and microwave measurements from a DPF had been considered as a feasible diagnostic [31]–[33] either on the inside or outside the vacuum chamber. Additionally, a dipole antenna was used by Escalona *et al.* [34] for measuring the electromagnetic noise created by the DPF and how to mitigate its effect in electronic equipment. Recently, a particular antenna design, the Vivaldi, has been used in conjunction with machine learning algorithms to infer the hard X ray measurement from DPF [35]. Despite the cited investigations reported the detection and described the behaviour of the EM burst from the DPF operation to some extent, no further intensity correlations with the commonly used electrical diagnostic signals, in particular the inductive measurement, were carried out using either hand-picked signal parameters or machine learning algorithms.

In the context of the use of a miniaturized DPF as a pulsed plasma accelerator, potentially for CubeSat propulsion, the aim of this work is to evaluate the replacement of the inductive sensor diagnostic of plasma focus with one done remotely using an antenna. Three tasks are presented to assess this proposal: the characterization of the DPF discharge using

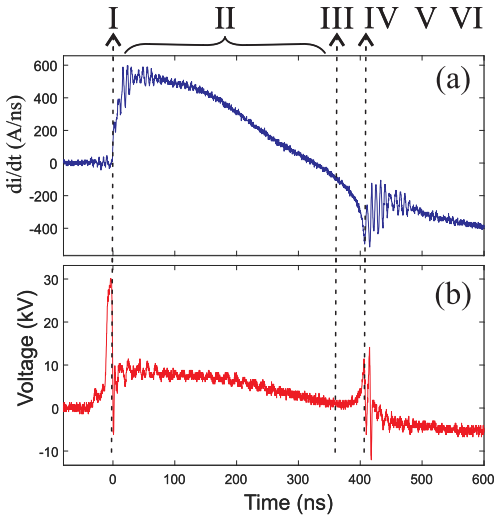

FIGURE 2. **Electric diagnostic of a DPF operation. (a) Rogowski coil and (b) voltage divider.**

the antenna signals in terms of the known inductive measurement, the identification of the transients from the antenna signals that are of interest to the proposed plasma focus application and the correlation of antenna signal parameters with the pinch detection feature from the inductive measurement signal. Measurements of a hundred of joules plasma focus operation, PF-400J [16], were carried out using an inductive sensor and three different antennas: monopole [36], Vivaldi [37] and helical [38]. To evaluate different antenna designs is relevant since they might serve, in a future work, to obtain the radiation pattern of an operational PPT based on the plasma focus type and thus get electromagnetic compatibility with other systems in the nanosatellite. Additionally, the use of different antennas was proposed to test which design obtained better correlation results. The adjusted coefficient of correlation R^2_{adj} was used to determine the best correlation result. Even tough in the case of a pulsed plasma thruster the discharge is produced in vacuum (the space conditions at the satellite orbit), two singular phenomena occur in a dense plasma focus discharge that produce a significant change in the current derivative which could be used in the remote diagnostic: the breakdown on the insulator (propellant) and the disruption plasma producing the ejected plasma shocks from the electrode gun. The electromagnetic behaviour (independent of the environment) and characterization of a plasma focus by means of inductive sensors and antennas, is believed to be a proper mimic of the expected behaviour in a pulsed plasma thruster of this kind for a nanosatellite.

II. ELECTRICAL DIAGNOSTIC, SENSOR CHARACTERISTICS AND EXPERIMENTAL SETUP

Examples of the Rogowski coil and voltage divider signals are shown in Fig. 2a and Fig. 2b, respectively. In stage **I**, the sudden fall of voltage is observed because of the dielectric breakdown of the gas which also indicates the start of the current increase, $di/dt > 0$. Stage **II** can be inferred to happen next. Stage **III** of radial compression of the plasma corresponds to an abrupt rise of its impedance [26], [39]. This behaviour is observed when the di/dt signal begins to decrease more sharply than the previous stage. The stagnation point is achieved at the pinch, stage **IV**, and is indicated by the dip in the di/dt signal and as a voltage surge in the voltage divider signal. The final stages, **V** and **VI**, cannot be directly observed using this electric diagnostic. After the pinch, the electrical signals follows the behaviour of an underdamped RLC series circuit. Note that high frequency oscillations are recorded when there are abrupt changes in current, stages **I** and **IV**, as suggested by Bruzonne *et al.* [40].

For a nanosatellite propulsion based on DPF architecture, it can be considered that the the initial stage **I** and pinch stage **IV** are of most interest for the diagnostic of the device operation. As was mentioned before, the detection of stage **I** indicates the start of the discharge process and then, the stage **IV**, the detection of the pinch which serves as an indicator of the abrupt changes in the circuit current due to the plasma dynamics.

The inductive sensor utilized in this study was an inductive loop sensor (ILS) [41], see Fig. 3a. This inductive sensor corresponds to one rectangular loop made in a circuit board and works in a similar way to a Rogowski coil. In this work, the ILS corresponds to the reference inductive signal where the already known physical phenomena of the discharge, such as the dip, can be identified. This sensor was previously developed for measuring fast varying current pulses from partial discharges [41], [42] and its constructional details are found in [43].

The antennas used in this study were: 22 cm monopole antenna [44], Vivaldi antenna [45] and helical antenna [38]. See, respectively, Fig. 3b, Fig. 3c and Fig. 3d. For the antennas, the S_{11} parameter, or reflection coefficient, is related to the antenna efficiency and is a key measure that is needed for evaluating the performance of an antenna when receiving far field components from the EM source. Antennas with high efficiency, for certain frequencies, present low reflection losses so it is common practice to consider values below of $S_{11} = -10$ dB as the frequencies where the antenna is adapted or tuned. Note that near field components (frequencies) can also be detected by the antennas [46]. For instance, according to the criteria indicated by the IEEE standard definition of terms for antennas [47], a region inside the boundary determined by $\frac{c}{2\pi f}$, where c is the speed of light and f a determined frequency, is considered a near field reactive region. The S_{11} measurement for each antenna was made with a vectorial network analyzer (VNA Master MS2035B) and its results are shown along with the detailed description of each sensor in the following list:

1) **Monopole antenna (22 cm)**: This omnidirectional antenna is one of the simplest antenna that can be constructed [44]. A copper wire with 1.6 mm diameter is attached to a BNC straight bulkhead socket (50 Ω). The length from the top of the conductor to the socket ground is 22 cm. Additionally, a 1.6 mm thickness and

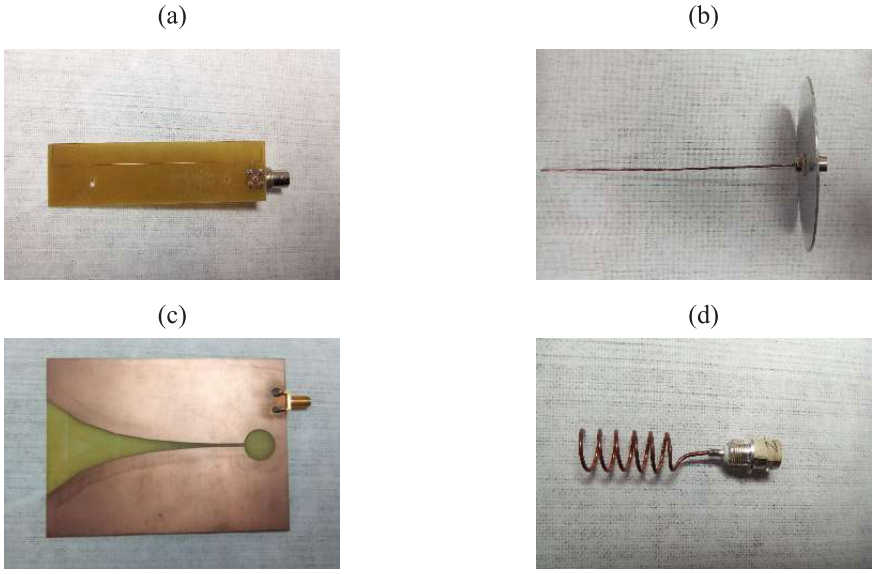

FIGURE 3. Picture of the sensors used: (a) inductive sensor loop, (b) Monopole antenna, (c) Vivaldi antenna and (d) helical antenna.

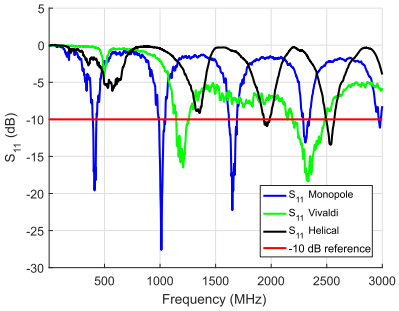

FIGURE 4. Measured S_{11} parameter for the antennas.

10 cm diameter aluminum circular plate is placed in the socket as a ground plane. The first resonant frequency of this antenna is calculated from the well known expression (1) [44] for a monopole with length L.

$$f = \frac{c}{4L} \tag{1}$$

The 22 cm monopole was designed to have the first resonance at 341 MHz. Fig. 4 shows the measured S_{11} parameter for this antenna in blue color. The first three resonances are located at 410 MHz, 1 GHz and 1.6 GHz. The differences between calculated and measured tuned frequencies are mainly due to the small ground plane, not infinite as equation (1) requires. In plasma focus EM burst measurement, a 30 cm long dipole (15 cm equivalent monopole) was previously used [34]. In this work, a longer monopole was proposed to test if the lower frequency emission detection, achieved better results in the correlation analysis. In contrast, a longer monopole is not suitable for the intended application of plasma focus for nanosatellite propulsion because its straight conductor could exceed size restrictions of the nanosatellite and also imposes a risk of undesired electric contact that could lead to shortcircuit. Despite these restrictions, it was worth to test and show its correlations results as is described in the result sections III-B.1 and III-B.2.

2) **Vivaldi antenna**: This antenna corresponds to a exponential slot line (waveguide) embedded in a substrate, where a micro-strip transmission line is used for getting the signal out to a SMA connector [45]. This type of antenna has a directional radiation pattern which means that, when it is directed towards the electromagnetic radiation source, the antenna receive the highest intensity, reducing at the same time the influence of other external sources and eventual reflections from conductive materials near the source. Because of the designed shape of the slot line, this antenna is adapted for a frequency band instead of a particular resonant frequency like the monopole. The properties of the Vivaldi have allowed this type of antenna to be useful in applications that requires bandwidth measurement of fast transient discharges [37], [48]. Recently, it proved to obtain good results for the inference of the hard X rays measurement signal from a plasma focus using a deep learning algorithm [35]. The Vivaldi antenna used in this study was made from a circuit board with dimensions 8.5 cm × 11.3 cm. The measured S_{11} parameter of the Vivaldi is shown in green color in Fig. 4. Although the frequency band between 1.2-2.3 GHz is not completely adapted, it still offers a bandwidth measurement mainly because the high power radiation emitted from DPF had been shown to be highly intense [34]. A less adapted peak around 500 MHz also allows for measuring near this frequency.

3) **Helical antenna**: This antenna is mainly chosen because of its axial radiation pattern [38] which allows a more directional receiving mode, thus minimizing the

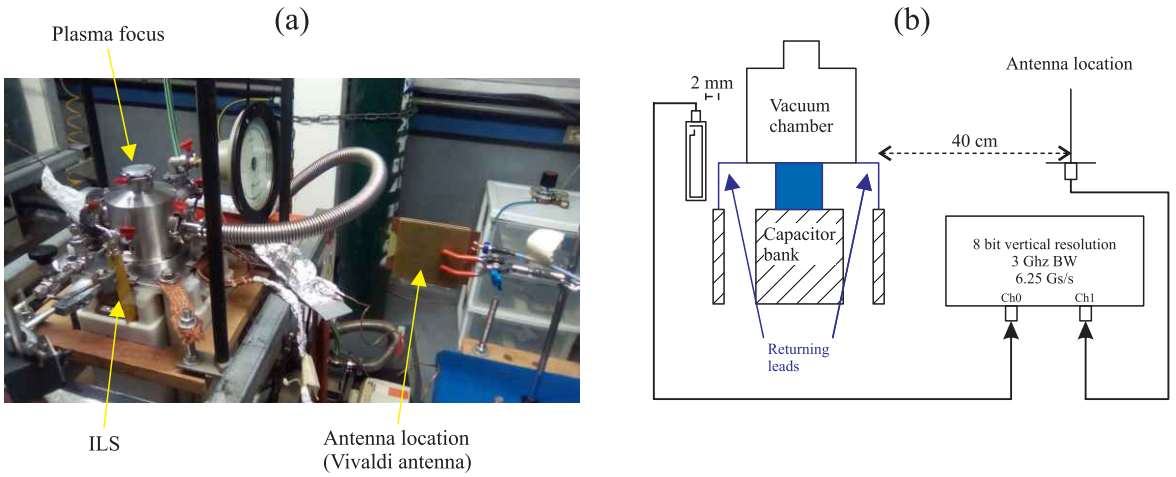

FIGURE 5. Sensor placement with respect to the DPF: (a) Experimental setup photo and (b) Layout. The inductive sensor loop is placed 2 mm from one of the return leads and the antennas were placed at 40 cm from another return lead.

detection of reflected waves from the surroundings of the DPF. This type of antenna was first developed by Kraus *et al.* [38], [49]. No previous applications of this antenna for EM burst measurements were found. The helical antenna was mounted in a 50 Ω BNC socket. No ground plane was provided for this antenna. The design parameters as described by Kraus are: 5.5 turns, 1.4 mm of conductor diammeter, 11.5 mm of helix diammeter, 6 mm of spacing between each turn and 15.75 mm of distance from the helix to the BNC socket. The S_{11} parameter measured for this antenna is shown in black color in Fig. 4. A first band of frequencies around 500 MHz and below are found to be sufficient for detecting the EM burst from the DPF despite of not satisfying the −10 dB criteria for adapted frequencies.

The measurements were taken from a low energy plasma focus PF-400J [16]. Parameters of this DPF are: 880 nF capacitor bank, 38 nH circuit inductance, 26 kV charging voltage, ≈ 287 J electrostatic energy and approximately 300 ns to maximum current. A modified electrode geometry with respect to the original one [16] was available. The modification consisted in the following: no cathode bars were placed for the external electrode, the insulator had an increased length of 21.5 mm and the effective length of the anode was 13 mm. The operational conditions for the experiment were set at 26 kV for charging voltage and the vacuum chamber was filled with pure hydrogen at a pressure of 9.5 mbar.

The experimental setup that indicate the location of the sensors with respect to the DPF is shown in Fig. 5a and its layout in Fig. 5b. The best alternative for placing the inductive sensor was at 2 mm from one of the return leads that connects the vacuum chamber to one of the capacitors. For the antennas, the closest return lead serves as reference point where a fixed distance of 0.4 m was chosen.

The acquisition system used for the measurements consisted in a PXI system which considers a NI-PXIe 1082 chassis, a NI-PXI 5162 acquisition card and a NI-PXIe-8115 controller with a dual-core i5-2510E processor. The measurement characteristics of the system are as follows: 2 channel, sampling frequency of 6.25 Gs/s, 3 GHz of bandwidth and 8-bit of vertical resolution. Attenuators of 20 dB and 30 dB with bandwidth of 0-18 GHz and 0-6 GHz, respectively, were used to keep high intensity signals in the range of 1 V_{pp} which is the maximum input limit for each channel (50Ω). The ILS signal was recorded in one channel, meanwhile the antenna signal was recorded in the other available channel as shown in Fig. 5b. The measurement campaign started with the simultaneous recording of the ILS and monopole signals, then the ILS with Vivaldi and, finally, with the ILS and helical. Each signal was recorded using a time window of 1 μs. A trigger unit was used to control the discharge of the spark-gap which was filled with pure nitrogen at a pressure of 0.5 bar. The repetitive trigger mode allowed the operation of the DPF on regular time intervals at the specified experimental conditions. A total of 200 discharges, with a 14 second interval between each one, were recorded for each ILS-antenna data set. Because of the stochastic and non-linear characteristics of plasma focus discharges, a diversity of diagnostic signals are obtained even when experimental conditions are the same: working gas, gas pressure, charging voltage and electrode geometry [25]. To validate that most of the differences in the antennas signals are due to their respective designs, the inductive loop sensor signals were analyzed. It was confirmed that the frequency content of the ILS in all data sets were almost identical.

III. RESULTS AND DISCUSSION

To evaluate the capability of the antennas to detect the stages of the discharge, a detailed analysis in time and frequency domain of the signals from each ILS-antenna data set is presented in Section III-A. The analysis was carried out by comparing the waveforms between the ILS and the antenna of a same discharge. The wavelet transform was also calculated to identify certain frequencies that appear during the discharge.

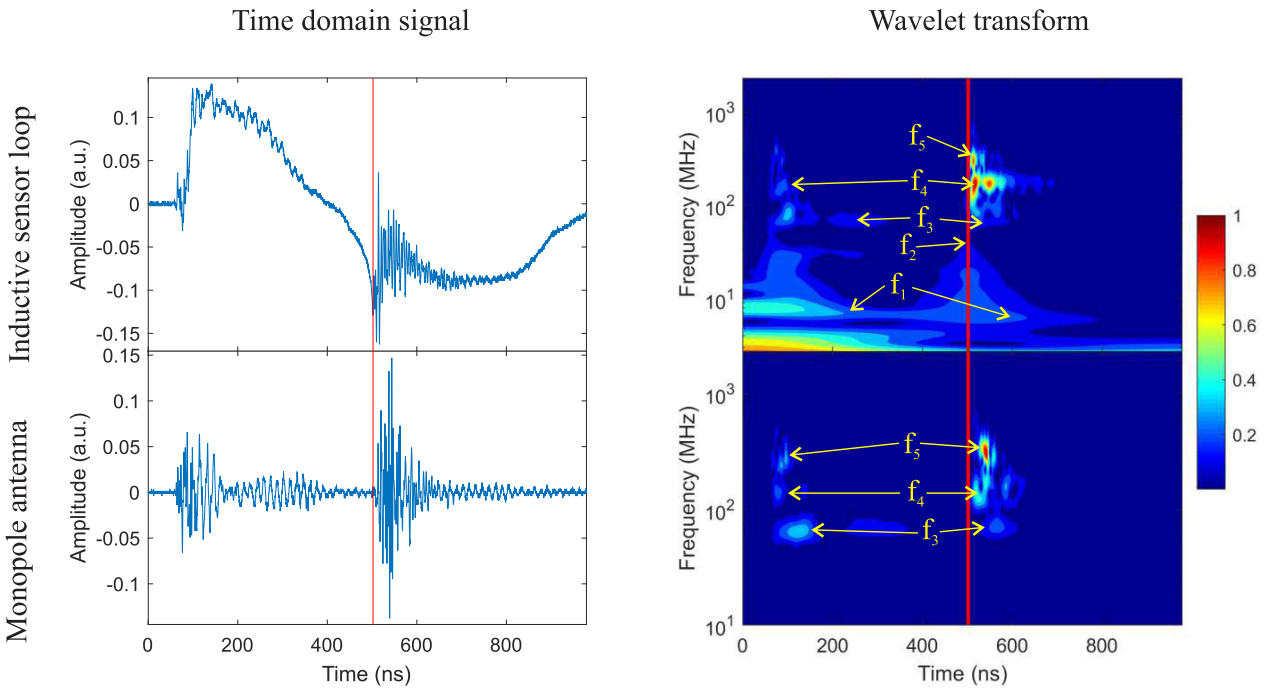

FIGURE 6. Measured signals and their wavelet transform for the ILS-Monopole comparison.

TABLE 1. Summary of the frequencies highlighted in the wavelet transform results from Figures 6, 7 and 8.

Frequencies of interest	**ILS** (MHz)	**Monopole** (MHz)	**Vivaldi** (MHz)	**Helical** (MHz)
f_1	6-7	—	—	—
f_2	≤ 50	—	—	≈ 30
f_3	≈ 70	≈ 70	≈ 70	≈ 70
f_4	120-200	110-190	140-230	120-210
f_5	250-350	250-370	—	—
f_6	—	—	340-510	220-530
f_7	—	—	670-1290	—

Furthermore, the correlation between the dip value feature of the ILS signal and the associated EM burst measured with antennas is investigated in section III-B. The correlations of the dip value from the ILS signal and the antennas signals were carried out using hand-picked parameters, such as signal energy and peak value, to represent the antenna signal. Additionally, correlations based on a frequency band energy calculation [50], were carried out to improve results of the previous correlations.

A. TIME AND FREQUENCY DOMAIN ANALYSIS OF THE MEASURED SIGNALS

First, the signals of the ILS and each respective antenna are shown in the time domain. For both sensors, the wavelet transform representation is also included for visualizing the frequency components that appear during the discharge. The use of the wavelet transform is adequate given that one of its applications is for detecting time-localized events in noisy signals [51] and, previously, it was used by Piriaei *et al.* [52] for analyzing the frequency content of electric signals measured from the DPF operation using a Mirnov coil.

The results for each ILS-antenna comparison are shown in Fig. 6 for the monopole case, Fig. 7 for the Vivaldi case and Fig. 8 for the helical case. One discharge example is shown for each case. The time domain signals are shown to the left of these three figures, meanwhile to the right are shown the wavelet transform results. Time of pinch is highlighted in the plot. For a better interpretation of the wavelet results, their coefficients were normalized by the maximum value of the respective transform, so values closer to one (red color) indicate a clear time-frequency identification. The wavelet transform results show that particular bands of frequencies were identified during the discharge in the ILS and antenna signals. Table 1 shows a summary of the frequency bands highlighted in the wavelet transform results from Fig. 6, Fig. 7 and Fig. 8. A description of each ILS-antenna comparison is shown next, along with the frequency details of each signal.

The ILS-monopole comparison shown in Fig. 6 indicates that the antenna detected two transients: the initial spark-gap conduction followed by the gas breakdown, stage **I**, and the later pinch, stage **IV**. Note that due to pinch an EM burst is detected by the antenna. This transient start to rise at time of

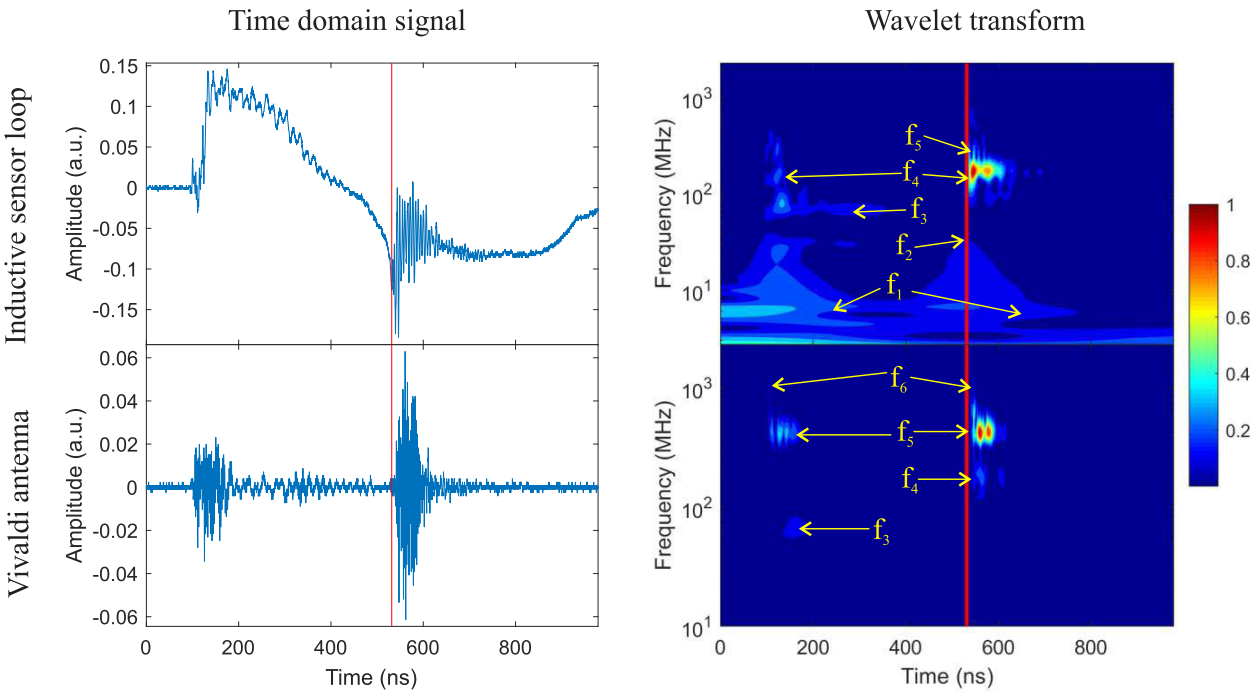

FIGURE 7. Measured signals and their wavelet transform for the ILS-Vivaldi comparison.

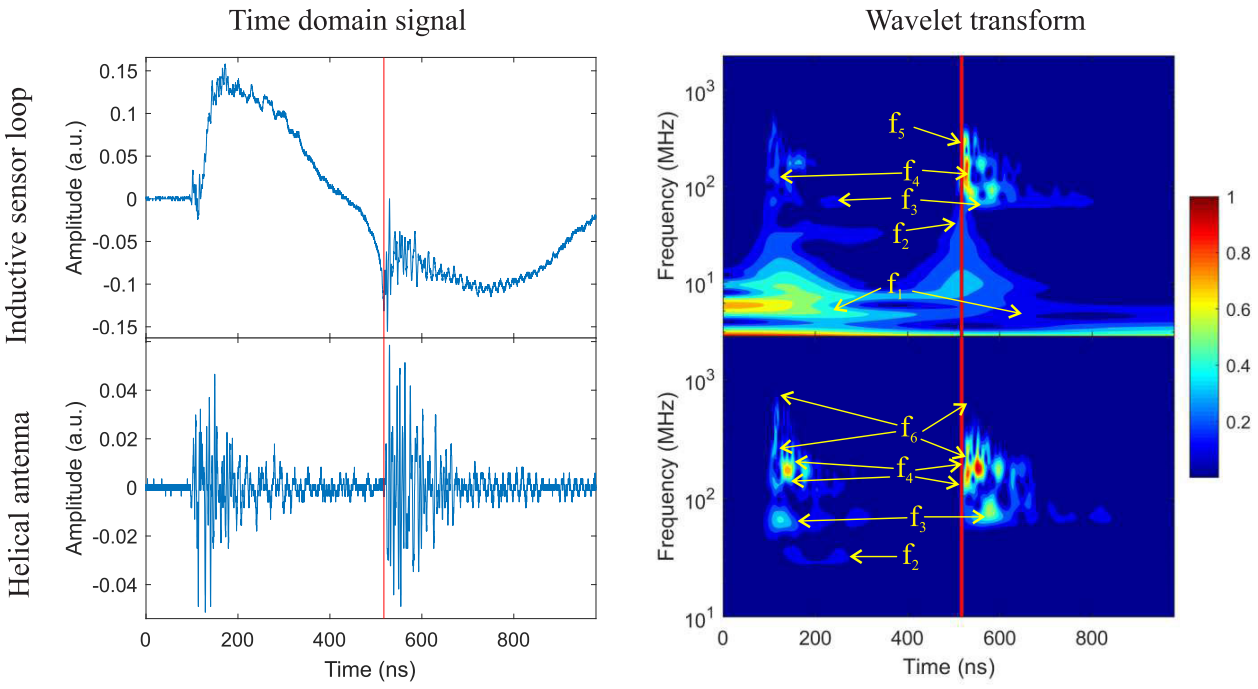

FIGURE 8. Measured signals and their wavelet transform for the ILS-Helical comparison.

pinch and shortly after reaches high amplitude oscillations, and then the transient decays.

The ILS spectrum consists mainly in five frequencies of interest, see Table 1: f_1 around 6-7 MHz that are present during most part of the discharge, f_2 shows a limit $\leq$ 50 MHz achieved during pinch stage, f_3 an oscillation of approximately 70 MHz during the initial stages and later in pinch stage, f_4 and f_5 are frequency bands that also appears mainly because of the abrupt changes in current in the initial stage and pinch. These frequency bands comprise 120-200 MHz and 250-350 MHz, respectively. f_4 and f_5 frequency bands are radiated components that are coupled into the ILS signal because this inductive sensor is not shielded from the EM burst [53]. In the ILS wavelet transform the lowest frequency

that can be identified corresponds to the main discharge frequency, i.e. the underdamped sinusoidal behaviour of the electrical circuit. This frequency is not highlighted in the wavelet transform results nor summarize in Table 1 because the antennas are not tuned for such low frequency value. Nevertheless, is worth noticing it as part of the electrical behaviour of the circuit. This frequency component can be approximately estimated (neglecting the damping due to the circuit resistance) with equation 2 [54]. This corresponds to the interaction between the capacitor bank (C_0) of 880 nF and the stray inductance (L_0) of 38 nH. The main discharge frequency is around 870 kHz which in turn is identified, with cyan color, at the bottom of ILS wavelet transform results during the entire discharge.

$$f_0 \approx \frac{1}{2\pi\sqrt{C_0 L_0}} = 870 \text{ kHz} \tag{2}$$

For the monopole antenna signal, see Fig. 6 and Table 1, three groups of frequency bands were identified. Those frequencies appear in the transient associated with pinch and also can be distinguished at the start of the discharge. A frequency around 70 MHz, f_3, appears during both transients and also at some part of the rundown stage. Its identification is overshadowed by higher frequency bands. The frequency band of 110-190 MHz, f_4, is present at the initial stages, but it is more clearly identified during pinch. The other high frequency band, f_5, lies between 250-370 MHz. Both f_4 and f_5 are detected at the initial transient and due to pinch. The highest frequency band, f_5, is remarkably identified in the transient associated with pinch and occurs a few tens of nanoseconds after it. Note that f_4 and f_5 are in similar ranges to the higher frequency bands detected by the ILS. This observation supports the idea that those components are coupled into the ILS signal rather than being part of the inductive measurement. In terms of the S_{11} parameter measured for the monopole antenna which has a first resonance (optimum) at 410 MHz, only f_5 is in the region where the antenna has the highest efficiency, although it is not optimized.

In the ILS-Vivaldi comparison, see Fig. 7, the Vivaldi antenna signal also identified the two transients previously detected by the monopole: initial spark-gap conduction/gas breakdown and pinch. The main difference is the frequency content observed by this antenna. The wavelet transform of the Vivaldi antenna signal shows that it contains four frequency bands, some of them the same as in the ILS and monopole. According to Table 1: f_3 correspond to approximately 70 MHz, similar to the monopole antenna, and is identified in the first transient; f_4 is a band found between 140-230 MHz and is mainly detected in the transient due to pinch; f_6 in the range of 340-510 MHz is notoriously present in both transients with major presence in the pinch transient; f_7, approximately 670-1290 MHz, shows a low presence of higher frequencies up to the GHz at both transients, but with short duration. This last high frequency band, f_7, is somewhat overshadowed in magnitude by lower frequency content such as the bands around 500 MHz that corresponds to the first valley from the S_{11} parameter, see section II. The difference in the frequency content relative to the monopole antenna was expected because the Vivaldi was tuned for different frequencies ($\approx$ 500 MHz and 1.2-2.3 GHz).

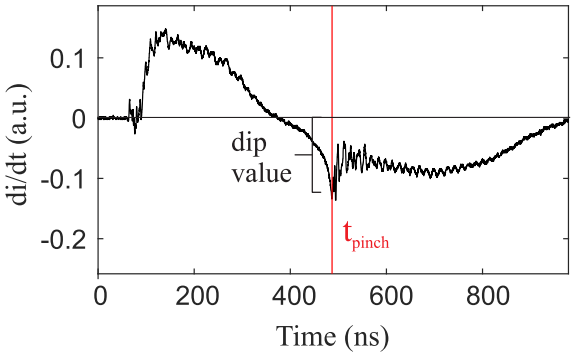

FIGURE 9. Example of the dip value parameter from the ILS signal.

In the ILS-helical comparison shown Fig. in 8, the time domain signal of the helical antenna shows that the two main transients are also detected. A slight difference is observed in the transient related to pinch. This transient starts immediately with high amplitude oscillations, in contrast to the monopole and Vivaldi measurement, where it was observed that this particular transient started at time of pinch and then its amplitude grew larger. The wavelet transform of the helical antenna visualizes this behaviour with the red areas noticeable at time of pinch and after. The frequencies of interest detailed in Table 1 are as follows: f_2 around 30 MHz at the transient related to the start of the discharge; f_3 around 70 MHz in both transients, similar to the previous cases; f_4 is in the range of 120-210 MHz in both transients, but more noticeable at pinch transient; f_6 a band of 220-530 MHz, also found in the pinch transient. These results indicate that both transients, measured with the helical antenna, are similar in shape and in frequency content. In terms of the S_{11} parameter of the helical antenna, the bands of frequencies, f_4 and f_6, correspond to those far field components that can be received more efficiently by this antenna.

B. CORRELATIONS BETWEEN THE INDUCTIVE AND RADIATED MEASUREMENTS

One of the most important characteristic of the inductive measurement is the dip value feature seen in the di/dt signal when the pinch occurs. This feature is related to the electromagnetic radiation and particle beam emission from DPF [13], [25]. It also serves to infer the plasma shock and plasma jets that are formed due to pinch. Because of its importance, the objective of this subsection is to search if the dip value from the ILS signal is correlated with the EM burst emitted from the DPF and measured with the antennas. This parameter corresponds to the ILS signal value at time of pinch. An example of the dip value parameter of the ILS signal is shown in Fig. 9.

For the antennas, the transient detected at time of pinch is considered as the EM burst measurement, thus neglecting

TABLE 2. Summary of fitted polynomials for the median value trend from Fig. 10. A growing trend of the median values with dip values is observed.

Comparison	Fit for median values			
	Peak value correlation		*Signal energy correlation*	
	Type	R^2_{adj}	*Type*	R^2_{adj}
ILS-Monopole	Linear polynomial ($p = 2$)	0.9658	Linear polynomial ($p = 2$)	0.9737
ILS-Vivaldi	Cubic polynomial ($p = 4$)	0.9633	Cubic polynomial ($p = 4$)	0.9257
ILS-Helical	Linear polynomial ($p = 2$)	0.9467	Linear polynomial ($p = 2$)	0.9517

the initial one for the correlations with the dip value. The EM transient considered correspond to the part of the antenna signal that starts at time of pinch until the end of the measurement, for example, see the helical antenna signal to the right of time of pinch in Fig. 8. Two complementary approaches are shown for correlating the EM burst with the dip value: first, parameters calculated from the time domain antenna signals, peak value and energy, are used for the correlation, and second, spectral energy of certain frequency bands from the FFT of the antenna transients is used.

1) PEAK VALUE AND SIGNAL ENERGY CORRELATION

The parameters calculated to represent the intensity of the time domain antenna signal were peak value and signal energy. Two parameters were chosen to verify if better correlations results were found with one parameter or both. Signal peak value has a straightforward interpretation related to the maximum amplitude oscillations obtained in the antenna signals. Signal energy gives a complementary information because it takes into consideration the whole transient for its calculation, equation 3 [55],

$$E_n = \sum_{i=1}^{n} v_i^2 \tag{3}$$

where E_n is the energy accumulated up to the n-th sample and v_i are the values of the antenna signal samples. The energy signal corresponds to the summation until the last sample of the transient.

The correlations are displayed using the boxplot representations. In this representation, the dip values were grouped and the antennas parameters corresponding to them were distributed accordingly. The boxplot was preferred over the scatter plot, parameter to parameter correlation, because no clear data trend was observed in the latter case. The results of the correlations between the ILS and each of the antennas are shown in Fig. 10.

Note that just the median value could be identified to have a clear increasing trend with dip values. This behaviour is highlighted with a red line that corresponds to a polynomial fit for the median values of each range. The results of the fits are shown in Table 2. The adjusted R-squared parameter R^2_{adj}, see equation 4 [56], is used for evaluating the fits that for instance can be linear, quadratic or cubic polynomials. In equation 4, n is the number of discharge measurements considered and p the number of parameters of the polynomial fit.

$$R^2_{adj} = 1 - \frac{(1 - R^2)(n - 1)}{n - p} \tag{4}$$

The increasing trend of median values is observed either by using the peak value or signal energy in each ILS-antenna comparison. In terms of the R^2_{adj} parameter for the median value fit, the best results are obtained by the monopole antenna using the signal energy parameter, i.e. the information of the whole transient seen by the antenna after pinch.

When analyzing the boxplots, see Fig. 10, high data dispersion is found along with the trend of the median values using either peak value or signal energy. Note that some of the discharges that produced the highest dips did not necessarily produced high value parameter in the antenna signal. At this point, no significant differences are observed by using a particular antenna, although the use of different tuned antennas allowed to identify the increasing trend of the EM burst with dip values.

2) FREQUENCY BAND ENERGY CORRELATION

A frequency domain approach is presented based on the results from the previous subsection. Again, the part of the signal considered was the transient after pinch. Previously, it was shown that the median value of either the peak values or signal energy had an increasing trend with dip values. The antenna signals associated to each median value from the peak values correlations, see Fig. 10-left, were selected and their fast Fourier transform (FFT) calculated.

The FFT results of each antenna are shown in Fig. 11-left. The FFT results are presented in terms of the dip value range to which the median value belongs to. This method for displaying the results is based on the visible spectroscopy diagnostic of plasma focus done by Feugeas and Grigioni [57].

Note that some frequencies exhibit an increasing trend with dip values whereas others do not. The frequency bands that follows this behaviour are highlighted in Fig. 11 left and summarized in the second column of Table 3. A final correlation was investigated using this observation by calculating the spectral energy from the FFT, using only the frequency bands that exhibited this trend. The frequency bands were selected by visual inspection, where each of them followed the increasing trend with dip values. The method of calculating signal energy using only particular frequency bands from the signal frequency spectrum, was based on the work of Ardila-Rey [50], a tool that was developed as a clustering technique for high frequency electrical signals. Equation 5 shows the calculation of the frequency band energy parameter,

$$E_{fb} = \sum_{i=1}^{N} \sum_{f=lf}^{hf} FFT^2(f) \tag{5}$$

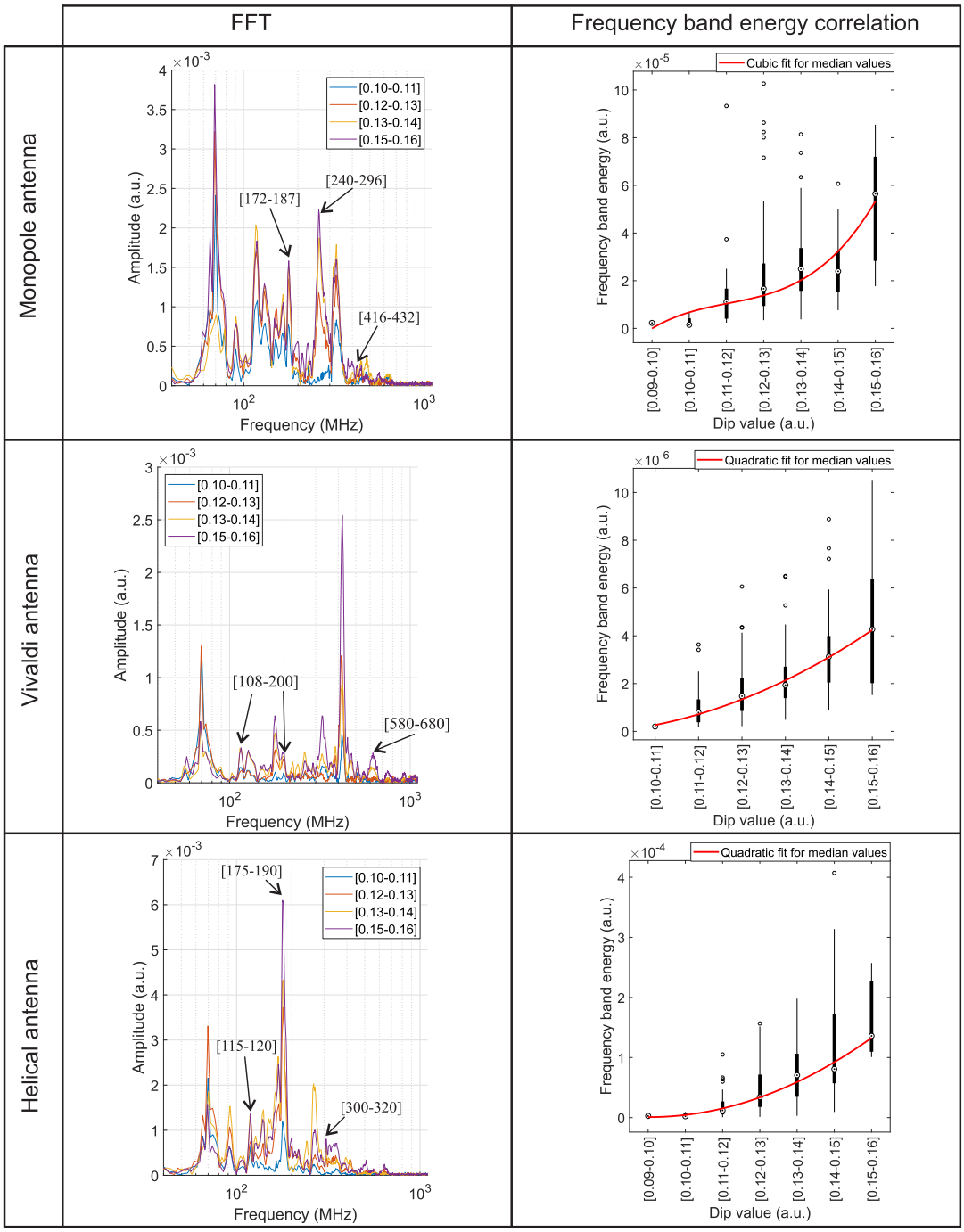

FIGURE 10. Correlations results between dip value and antenna signal parameters from the transient due to pinch: To the left the correlations using the peak value and to the right the correlations using signal energy. Each row correspond to an ILS-antenna data set.

where E_{fb} is the frequency band energy, the summation is over the N numbers of selected frequency bands of interest and in each frequency band the summation is done from lf, the lower limit of it, to hf, the high frequency limit of the band.

The correlations results between frequency band energy and dip values are shown in Fig. 11. The increasing trend of the median values with dip values is also observed by this correlation. The adjusted polynomials for median values are highlighted in red in Fig. 11-right. The details of the fits are shown in Table 3. Note that for the cases using a Vivaldi or helical antenna the trend is more visible than the results using peak values and signal energy, although data dispersion with respect to the fitted polynomials still persists. For the Vivaldi and helical cases it was found that the median values followed a quadratic trend, having the Vivaldi result the highest R^2_{adj} parameter. The lowest R^2_{adj} parameter for the median value

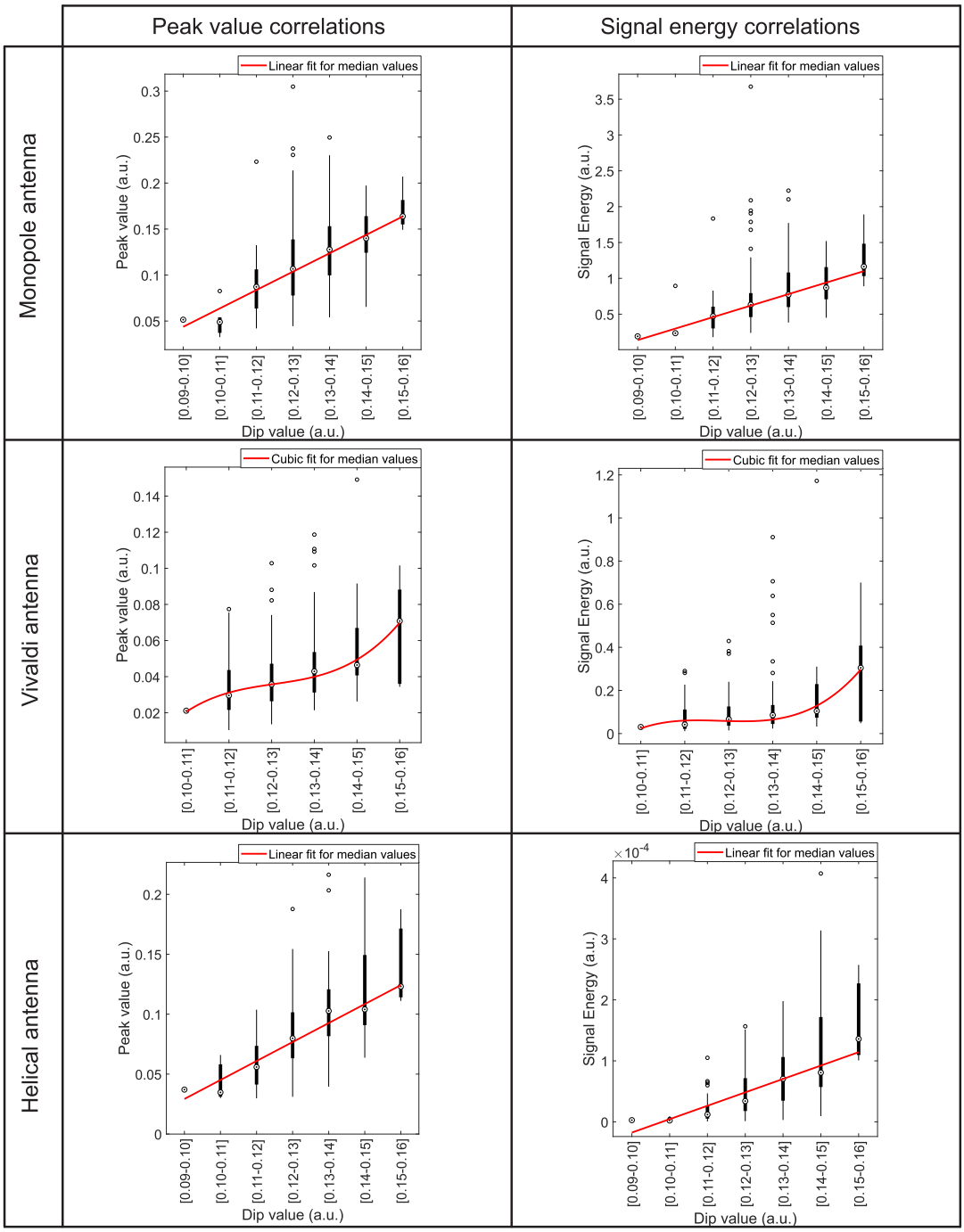

FIGURE 11. Correlations based on the frequency content of the antenna signal: The left column corresponds to the FFT of four discharges associated to the median values from the peak value correlations in Fig. 10 and the frequencies that exhibit a growing trend with dip values. The right column shows the correlations using the frequency band energy parameter. The polynomial fit of the median values is highlighted with red color. Each row correspond to an ILS-antenna data set.

fit was obtained in the monopole case. A cubic fit was more suitable than the linear fit as was informed in the previous Table 2. High data dispersion with respect to the fit was also found for the monopole case.

C. DISCUSSION

Time derivative of current, di/dt, is one of the mechanism for electromagnetic radiation from conductors [44], [58]. The structure itself of the DPF is acting like an emitting antenna as was first described by Gerdin *et al.* [33]. According to the results presented in section III-A, all three antenna signals detected two transients that can be associated with important stages of the discharge where high values of di/dt were detected by the inductive measurement:

1) Stage **I**: The first transient is associated to a EM burst which can be traced back to the spark-gap conduction

TABLE 3. Summary of the frequency bands selected and correlations results from Fig. 11.

Comparison	Selected frequency bands for the spectral energy calculation $[lf - hf]$ (MHz)	Polynomial fit for mean values	
		Type	R^2_{adj}
ILS-Monopole	172-187 240-296 416-432	Cubic ($p = 4$)	0.8643
ILS-Vivaldi	106-200 580-680	Quadratic ($p = 3$)	0.9901
ILS-Helical	115-120 175-190 300-320	Quadratic ($p = 3$)	0.9707

and initial gas breakdown. These two events occur at the start of the discharge. First, the spark-gap conduction that allows the high voltage connection to the anode and then the gas breakdown inside the chamber.

2) Stage **IV**: The second transient can be time correlated to pinch. This particular event seems to be related to a switching action phenomena as predicted by Bruzzone *et al.* [40]. High frequency components are excited again, after the initial stage of the discharge, as can be seen in the inductive and antennas signals at time of pinch. The transients detected by the antennas support this claim, particularly, the wavelet transforms indicate that the frequency content of the transients, initial and pinch, do not differ significantly, so it can be concluded that the radiated frequencies are excited again due to the discharge process. Similar EM bursts during pinch and after it was observed by Gerdin *et al.* [33] and Escalona *et al.* [34] using other antennas and measurement methods.

Despite the continuous time variation of current, not all stages of the discharge can be time correlated clearly with respect to the inductive measurement. However, for the possible application of DPF as a propulsion system of nanosatellites, the identification of the mentioned stages (**I** and **IV**) is sufficient for assuring the beginning of the discharge and latter formation of dense plasma.

Two approaches, using signal parameters from either the time or frequency domain representation of the signal, were presented. When the antenna data results were grouped in terms of dip value, as was presented in their respective boxplot, a clear increasing trend for their median values was identified with all antennas. Although the antennas were different, this result is consistent with the fact that this behavior was seen by all of them. Data dispersion, with respect to the median value trend, was found with all antennas, and thus, a variety of measured EM bursts were obtained from the DPF operation. Using the time domain representation, with either peak values and signal energy, the monopole antenna achieved better results in terms of the R^2_{adj} parameter. As detailed in section II, size restrictions limit the use of large monopole antennas. Nonetheless, the measured correlation enable its use as a remote sensor for plasma focus operation characterization. From the other sensors, the Vivaldi achieved better results using the peak value representation. The approach using the frequency band energy parameter for the representation of the EM burst measured with the antennas yielded slightly different results. In this case, the better results of the monopole could not be replicated. Outlier data were still found for medium dip values. For instance, see the cases where the higher signal parameters were associated with medium range dip values, the range of [0.12-0.14] (a.u.), instead of the highest dip values in the range of [0.15-0.16] (a.u.), see the monopole case in Fig. 11-right. With the frequency domain approach, the use of directional antennas, Vivaldi and helical antenna, seems more suitable for measuring the dense plasma focus operation, see their R^2_{adj} parameters from Table 3. In particular, the highest value of the R^2_{adj} parameter for the median value trend was achieved with the Vivaldi antenna. Moreover, the ILS-Vivaldi correlation showed that the highest frequency band energy parameter was associated to a highest dip value, see the Vivaldi case in Fig. 11-right. In contrast, the ILS-helical comparison showed some high value parameters associated to medium dip values such as the range [0.14-0.15] (a.u.) instead to the highest dip value range, see the helical case in Fig. 11-right. Directional antennas can potentially enable the electromagnetic compatibility study of the DPF when used as a thruster, since it facilitates the determination of the preferred direction of the radiated electromagnetic signals from the DPF. Along with the a deeper study of the plasma focus as a PPT, the electromagnetic compatibility of the device will be carried out in future work.

Three regions can be defined for the electromagnetic phenomena [46], [47]: reactive near field, radiating near field (Fresnel) and far field (Fraunhofer). The DPF, as an emitting antenna, can thus produce frequency components that fall in those regions. Considering the location of the antennas from the DPF, 0.4 m in this work, diverse frequency spectrums, including frequencies different from the S_{11} measurement, were obtained for all antennas, see Fig. 11-left. Some reactive near field components were present (reactive coupling) in all antenna signals, see the frequencies of interest from the wavelet transform results in Table 1. The frequency spectrum approach presented, indicate that some frequency bands that aided to improve correlation results, were not in the bands that the antennas were tuned, see Fig. 4. It can be deduced from the frequency band correlation results that, in addition to the far field components, reactive near field

components carry information as well. The near field components cannot be discarded in the analysis because, in the proposed application for the DPF, the antennas must be placed near it. It is a combination of information from the far and near field components that correlates better with the dip value intensity. Different electric parameters and device geometry will produce a different frequency spectrum, which presents an opportunity to apply machine learning algorithms to find the required spectral information. For example, to search for the frequency bands that the clustering technique from which this work is based on [50], a particle swarm optimization [59] was recently developed.

For the moment, the identification of the frequency components and their relationship with the physical phenomena occurring inside the plasma column, is not understood. It is known from the works of Bruzzone *et al.* [40], [54] that high frequency oscillations in the electrical signals can be explained as interactions of energy flows between capacitances, the capacitor bank and the stray ones, and inductances conformed by the plasma inside the chamber and stray inductance from the conductor leads. The study of these frequencies related to the electric parameters of the DPF and their capacity to be radiated will be considered in future work.

IV. CONCLUSION

The experimental results of antennas for measuring the electromagnetic bursts from the dense plasma focus operation were presented. The use of antennas was proposed for a non invasive diagnostic of the dense plasma focus operation as a pulsed plasma thruster for the propulsion system of a nanosatellite. Two phenomena associated with the discharge were identified as the crucial ones to be detected by this diagnostic: the initial dielectric breakdown and plasma pinch formation (including its later disruption). The important phenomena of plasma disruption after pinch is inferred based on the dip feature observed in an inductive sensor. This fact was used to relate the respective transient observed in the antenna signal and correlate it to the inductive measurement. Data dispersion was found in the correlations, which encourages further research on the electromagnetic radiation emitted from dense plasma focus devices. Correlations using the peak value and signal energy of the antenna signal yielded better results in the monopole case. Of the other designs, the Vivaldi antenna using the peak value parameter obtained good results, only slightly below the monopole ones. Using a frequency spectrum criteria, the correlation results of the Vivaldi and helical antennas were improved. The Vivaldi antenna achieved the best results using this frequency band correlation. The main conclusion of the frequency approach presented is that the information in the frequency domain can achieve better results in finding a correlation with the dip value of an inductive sensor. Considering the projected miniaturization of a plasma focus intended to be used as a pulsed plasma thruster in a nanosatellite, a Vivaldi patch antenna represents a feasible alternative that can replace an inductive sensor measurement.

ACKNOWLEDGMENT

The authors thank Dr. Sergio Davis for his suggestions and comments about the statistical analysis of the data.

REFERENCES

[1] H. Heidt, J. Puig-Suari, A. Moore, S. Nakasuka, and R. Twiggs, "CubeSat: A new generation of picosatellite for education and industry low-cost space experimentation," in *Proc. Annu. Conf. Events Small Satell.*, 2000, pp. 1–19.

[2] J. Puig-Suari, C. Turner, and W. Ahlgren, "Development of the standard cubesat deployer and a cubesat class picosatellite," in *Proc. IEEE Aerosp. Conf. Proc.*, vol. 1, Mar. 2001, pp. 1/347–1/353.

[3] C. Boshuizen, J. Mason, P. Klupar, and S. Spanhake, "Results from the planet labs flock constellation," in *Proc. Conf. Event Small Satell.*, Aug. 2014, pp. 1–8. [Online]. Available: https://digitalcommons.usu.edu/smallsat/2014/PrivEnd/1

[4] M. A. Diaz, J. C. Zagal, C. Falcon, M. Stepanova, J. A. Valdivia, M. Martinez-Ledesma, J. Diaz-Peña, F. R. Jaramillo, N. Romanova, E. Pacheco, M. Milla, M. Orchard, J. Silva, and F. P. Mena, "New opportunities offered by Cubesats for space research in Latin America: The SUCHAI project case," *Adv. Space Res.*, vol. 58, no. 10, pp. 2134–2147, 2016.

[5] National Academies Sciences, Medicine, *Achieving Science with CubeSats Thinking Inside the Box*. Washington, DC USA: National Academies Press, 2016.

[6] R. J. Barnett, "Oneweb non-geostationary satellite system: Technical information to supplement schedules—Attachment to fcc application satloi-20160428-00041," Federal Commun. Commission, Washington, DC, USA, Tech. Rep. SAT-LOI-20160428-00041, 2016. [Online]. Available: https://fcc.report/IBFS/SAT-LOI-20160428-00041/1134939.pdf

[7] M. Albulet, "Spacex non-geostationary satellite system: Technical information to supplement schedules—Attachment to fcc application satloa-20161115-00118," Federal Commun. Commission, Washington, DC, USA, Tech. Rep. SAT-LOA-20161115-00118, 2016. [Online]. Available: https://fcc.report/IBFS/SAT-LOA-20161115-00118/1158350.pdf

[8] National Academies Sciences Medicine, *NASA Space Technology Roadmaps and Priorities Revisited*. Washington, DC USA: National Academies Press, 2016.

[9] A. R. Tummala and A. Dutta, "An overview of cube-satellite propulsion technologies and trends," *Aerospace*, vol. 4, no. 4, p. 58, 2017. [Online]. Available: http://www.mdpi.com/2226-4310/4/4/58

[10] I. Levchenko, K. Bazaka, Y. Ding, Y. Raitses, S. Mazouffre, T. Henning, P. J. Klar, S. Shinohara, J. Schein, L. Garrigues, M. Kim, D. Lev, F. Taccogna, R. W. Boswell, C. Charles, H. Koizumi, Y. Shen, C. Scharlemann, M. Keidar, and S. Xu, "Space micropropulsion systems for Cubesats and small satellites: From proximate targets to furthermost frontiers," *Appl. Phys. Rev.*, vol. 5, no. 1, 2018, Art. no. 011104.

[11] L. Soto, C. Pavez, A. Tarifeño, J. Moreno, and F. Veloso, "Studies on scalability and scaling laws for the plasma focus: Similarities and differences in devices from 1 MJ to 0.1 J," *Plasma Sources Sci. Technol.*, vol. 19, no. 5, 2010, Art. no. 055017.

[12] S. Lee and A. Serban, "Dimensions and lifetime of the plasma focus pinch," *IEEE Trans. Plasma Sci.*, vol. 24, no. 3, pp. 1101–1105, Jun. 1996.

[13] L. Soto, "New trends and future perspectives on plasma focus research," *Plasma Phys. Controlled Fusion*, vol. 47, no. 5, p. A361, 2005.

[14] M. G. Haines, S. V. Lebedev, J. P. Chittenden, F. N. Beg, S. N. Bland, and A. E. Dangor, "The past, present, and future of *Z* pinches," *Phys. Plasmas*, vol. 7, no. 5, pp. 1672–1680, 2000.

[15] C. Pavez, J. Pedreros, M. Zambra, F. Veloso, J. Moreno, T.-S. Ariel, and L. Soto, "Potentiality of a small and fast dense plasma focus as hard X-ray source for radiographic applications," *Plasma Phys. Controlled Fusion*, vol. 54, no. 10, 2012, Art. no. 105018.

[16] P. Silva, J. Moreno, L. Soto, L. Birstein, R. E. Mayer, and W. Kies, "Neutron emission from a fast plasma focus of 400 joules," *Appl. Phys. Lett.*, vol. 83, no. 16, pp. 3269–3271, 2003.

[17] L. Soto, C. Pavez, J. Moreno, M. Cárdenas, A. Tarifeño, P. Silva, M. Zambra, L. Huerta, C. Tenreiro, J. L. Giordano, M. Lagos, C. Retamal, R. Escobar, J. Ramos, and L. Altamirano, "Dense transient pinches and pulsed power technology: Research and applications using medium and small devices," *Phys. Scripta*, vol. T131, Dec. 2008, Art. no. 014031.

[18] L. Soto, C. Pavéz, J. Moreno, L. Altamirano, L. Huerta, M. Barbaglia, A. Clausse, and R. E. Mayer, "Evidence of nuclear fusion neutrons in an extremely small plasma focus device operating at 0.1 joules," *Phys. Plasmas*, vol. 24, no. 8, 2017, Art. no. 082703.

[19] L. Soto, P. Silva, J. Moreno, M. Zambra, W. Kies, R. E. Mayer, A. Clausse, L. Altamirano, C. Pavez, and L. Huerta, "Demonstration of neutron production in a table-top pinch plasma focus device operating at only tens of joules," *J. Phys. D, Appl. Phys.*, vol. 41, no. 20, 2008, Art. no. 205215.

[20] L. Soto, C. Pavez, J. Moreno, M. J. Inestrosa-Izurieta, F. Veloso, G. Gutiérrez, J. Vergara, A. Clausse, H. Bruzzone, F. Castillo, and L. F. Delgado-Aparicio, "Characterization of the axial plasma shock in a table top plasma focus after the pinch and its possible application to testing materials for fusion reactors," *Phys. Plasmas*, vol. 21, no. 12, 2014, Art. no. 122703.

[21] M. J. Inestrosa-Izurieta, E. Ramos-Moore, and L. Soto, "Morphological and structural effects on tungsten targets produced by fusion plasma pulses from a table top plasma focus," *Nucl. Fusion*, vol. 55, no. 9, 2015, Art. no. 093011.

[22] J. L. Ellsworth, S. Falabella, V. Tang, A. Schmidt, G. Guethlein, S. Hawkins, and B. Rusnak, "Design and initial results from a kilojoule level dense plasma focus with hollow anode and cylindrically symmetric gas puff," *Rev. Sci. Instrum.*, vol. 85, no. 1, 2014, Art. no. 013504.

[23] J. Jain, J. Moreno, R. Andaur, R. Armisen, D. Morales, K. Marcelain, G. Avaria, B. Bora, S. Davis, C. Pavez, and L. Soto, "Hundred joules plasma focus device as a potential pulsed source for *in vitro* cancer cell irradiation," *AIP Adv.*, vol. 7, no. 8, 2017, Art. no. 085121.

[24] J. W. Mather, "15. Dense plasma focus," *Methods Exp. Phys.*, vol. 9, pp. 187–249, Jan. 1971.

[25] A. Bernard, H. Bruzzone, P. Choi, H. Chuaqui, V. Gribkov, J. Herrera, K. Hirano, A. Krejci, S. Lee, C. Luo, and F. Mezzetti, "Scientific status of plasma focus research," *J. Moscow Phys. Soc.*, vol. 8, pp. 93–170, Nov. 1998.

[26] F. Veloso, C. Pavez, J. Moreno, V. Galaz, M. Zambra, and L. Soto, "Correlations among neutron yield and dynamical discharge characteristics obtained from electrical signals in a 400 J plasma focus," *J. Fusion Energy*, vol. 31, no. 1, pp. 30–37, 2012.

[27] J. Jain, J. Moreno, D. Morales, S. Davis, B. Bora, G. Avaria, M. J. Inestrosa-Izurieta, and L. Soto, "Observation and interpretation of neutron origin prior to hard X rays and pinch in a hundred joules plasma focus device," *Laser Part. Beams*, vol. 35, pp. 656–662, Dec. 2017.

[28] C. Pavez, J. Pedreros, A. Tarifeño-Saldivia, and L. Soto, "Observation of plasma jets in a table top plasma focus discharge," *Phys. Plasmas*, vol. 22, no. 4, 2015, Art. no. 040705.

[29] D. G. Pellinen, Q. Johnson, and A. Mitchell, "A picosecond risetime high voltage divider," *Rev. Sci. Instrum.*, vol. 45, no. 7, pp. 944–946, 1974.

[30] A. Harper, M. Ryschkewitsch, A. Obenschain, and R. Day, "General environmental verification standard (gevs) for gsfc flight programs and projects," NASA Goddard Space Flight Center, Greenbelt, MD. USA, Tech. Rep., GSFC-STD-7000, 2005.

[31] J. L. Ellsworth, S. Falabella, A. Schmidt, and V. Tang, "Ion beam and neutron output from a sub-kilojoule dense plasma focus," *AIP Conf. Proc.*, vol. 1639, no. 1, pp. 27–30, 2014.

[32] A. Schmidt, A. Link, D. Welch, J. Ellsworth, S. Falabella, and V. Tang, "Comparisons of dense-plasma-focus kinetic simulations with experimental measurements," *Phys. Rev. E, Stat. Phys. Plasmas Fluids Relat. Interdiscip. Top.*, vol. 89, no. 6, 2014, Art. no. 061101.

[33] G. Gerdin, M. J. Tanis, and F. Venneri, "Observation of microwave emission from a plasma focus at frequencies well below the mean plasma frequency," *Plasma Phys. Controlled Fusion*, vol. 28, no. 3, pp. 527–545, 1986.

[34] I. Escalona, G. Avaria, M. Díaz, J. Ardila-Rey, J. Moreno, C. Pavez, and L. Soto, "Electromagnetic burst measurement system based on low cost UHF dipole antenna," *Energies*, vol. 10, no. 9, p. 1415, 2017.

[35] G. Avaria, J. Ardila-Rey, S. Davis, L. Orellana, B. Cevallos, C. Pavez, and L. Soto, "Hard X-ray emission detection using deep learning analysis of the radiated UHF electromagnetic signal from a plasma focus discharge," *IEEE Access*, vol. 7, pp. 74899–74908, 2019.

[36] G. Robles, J. M. Martínez-Tarifa, M. Rojas-Moreno, R. Albarracín, and J. Ardila-Rey, "Antenna selection and frequency response study for UHF detection of partial discharges," in *Proc. IEEE Int. Instrum. Meas. Technol. Conf.*, May 2012, pp. 1496–1499.

[37] G. Robles, R. Albarracín, J. L. Vázquez-Roy, E. Rajo-Iglesias, J. M. Martínez-Tarifa, M. V. Rojas-Moreno, M. Sánchez-Fernández, and J. Ardila-Rey, "On the use of Vivaldi antennas in the detection of partial discharges," in *Proc. IEEE Int. Conf. Solid Dielectr. (ICSD)*, Jun./Jul. 2013, pp. 302–305.

[38] J. Kraus and R. Marhefka, *Antennas For All Applications*, 2nd ed. New York, NY, USA: McGraw-Hill, 2002. [Online]. Available: http://adsabs.harvard.edu/abs/2002aaa.book...K

[39] H. Bruzzone, H. Acuña, M. Barbaglia, and A. Clausse, "A simple plasma diagnostic based on processing the electrical signals from coaxial discharges," *Plasma Phys. Controlled Fusion*, vol. 48, no. 5, p. 609, 2006.

[40] H. Bruzzone, H. Kelly, and C. Moreno, "The effect of transmission lines and switching action on the electrical signals in a powerful capacitive discharge," *IEEE Trans. Plasma Sci.*, vol. 18, no. 4, pp. 689–694, Aug. 1990.

[41] G. Robles, J. M. Martinez-Tarifa, M. V. Rojas-Moreno, and J. Sanz-Feito, "Inductive sensor for measuring high frequency partial discharges within electrical insulation," *IEEE Trans. Instrum. Meas.*, vol. 58, no. 11, pp. 3907–3913, Nov. 2009.

[42] M. V. Rojas-Moreno, G. Robles, J. M. Martínez-Tarifa, and J. Sanz-Feito, "Self-integrating inductive loop for measuring high frequency pulses," *Rev. Sci. Instrum.*, vol. 82, no. 8, 2011, Art. no. 085102.

[43] J. A. Ardila-Rey, A. Barrueto, A. Zerene, B. A. de Castro, J. A. C. Ulson, A. A. Mas'ud, and P. Valdivia, "Behavior of an inductive loop sensor in the measurement of partial discharge pulses with variations in its separation from the primary conductor," *Sensors*, vol. 18, no. 7, p. 2324, 2018. [Online]. Available: http://www.mdpi.com/1424-8220/18/7/2324

[44] C. A. Balanis, *Antenna Theory Analysis and Design*, vol. 28. Hoboken, NJ, USA: Wiley, 2012.

[45] P. Gibson, "The Vivaldi aerial," in *Proc. 9th Eur. Microw. Conf.*, Sep. 1979, pp. 101–105.

[46] C. A. Balanis, "Antenna theory: A review," *Proc. IEEE*, vol. 80, no. 1, pp. 7–23, Jan. 1992.

[47] "IEEE standard definitions of terms for antennas," *IEEE Trans. Antennas Propag.*, vol. 17, no. 3, pp. 262–269, May 1969.

[48] R. Albarracin, G. Robles, J. M. Martinez-Tarifa, and J. Ardila-Rey, "Separation of sources in radiofrequency measurements of partial discharges using time—Power ratio maps," *ISA Trans.*, vol. 58, pp. 389–397, Sep. 2015. doi: 10.1016/j.isatra.2015.04.006

[49] J. D. Kraus, "Helical beam antennas for wide-band applications," *Proc. IRE*, vol. 36, no. 10, pp. 1236–1242, Oct. 1948.

[50] J. A. Ardila-Rey, J. M. Martínez-Tarifa, G. Robles, and M. V. Rojas-Moreno, "Partial discharge and noise separation by means of spectral-power clustering techniques," *IEEE Trans. Dielectr. Electr. Insul.*, vol. 20, no. 4, pp. 1436–1443, Aug. 2013.

[51] J. M. Lilly, "Element analysis: A wavelet-based method for analysing time-localized events in noisy time series," *Proc. Roy. Soc. A, Math. Phys. Eng. Sci.*, vol. 473, no. 2200, 2017, Art. no. 20160776.

[52] D. Piriaei, T. Mahabadi, S. Javadi, and M. Ghoranneviss, "The effects of the cathode array on emitted hard X-ray from a small plasma focus device," *Phys. Plasmas*, vol. 24, no. 8, 2017, Art. no. 083508.

[53] J. A. Ardila-Rey, J. Montaña, B. A. De Castro, R. Schurch, J. A. C. Ulson, F. Muhammad-Sukki, and N. A. Bani, "A comparison of inductive sensors in the characterization of partial discharges and electrical noise using the chromatic technique," *Sensors*, vol. 18, no. 4, p. 1021, 2018.

[54] H. Bruzzone, H. Acuña, M. Barbaglia, M. Milanese, and A. Clausse, "Stray capacitance in a plasma focus device: Implications on the current derivative calibration and the effective discharge current," *J. Fusion Energy*, vol. 36, nos. 2–3, pp. 87–91, 2017.

[55] R. C. Guido, "A tutorial on signal energy and its applications," *Neurocomputing*, vol. 179, pp. 264–282, Feb. 2016.

[56] J. M. Martínez-Tarifa, G. Robles, and M. A. Hombrados-Herrera, "Ageing study on enameled magnet wires through statistical analysis of conventional partial discharge magnitudes and repetition rate," in *Proc. IEEE Int. Conf. Dielectr. (ICD)*, vol. 2, Jul. 2016, pp. 650–653.

[57] J. Feugeas and G. Grigioni, "Optical emission spectroscopy of electrical focii discharges," *J. Phys. D, Appl. Phys.*, vol. 30, no. 14, p. 2026, 1997.

[58] E. K. Miller and J. A. Landt, "Direct time-domain techniques for transient radiation and scattering from wires," *Proc. IEEE*, vol. 68, no. 11, pp. 1396–1423, Nov. 1980.

[59] G. Robles, J. M. Fresno, J. M. Martínez-Tarifa, J. A. Ardila-Rey, and E. Parrado-Hernández, "Partial discharge spectral characterization in HF, VHF and UHF bands using particle swarm optimization," *Sensors*, vol. 18, no. 3, p. 746, 2018.

LUIS ORELLANA was born in San Fernando, Chile, in 1992. He received the B.S. degree in electrical engineering from Federico Santa María Technical University, in 2015, where he is currently pursuing the M.S. degree in electrical engineering.

Since 2018, he has been working in the thesis about the Relationship Between the Electromagnetic Burst from Dense Plasma Focus and other diagnostics of the device, with the Plasma and Nuclear Fusion Laboratory, Comisión Chilena de Energía Nuclear. His research interests include the application of high voltage techniques to pulsed power devices and signal analysis.

JORGE ARDILA was born in Santander, Colombia, in 1984. He received the B.Sc. degree in mechatronic engineering from the Universidad de Pamplona, Pamplona, Colombia, in 2007, the Specialist Officer degree in naval engineering from Escuela Naval Almirante Padilla, Cartagena, Colombia, in 2008, and the M.Sc. and Ph.D. degrees in electrical engineering from the Universidad Carlos III de Madrid (UC3M), in 2012 and 2014, respectively. He was an Automatic Control Engineer of ARC Almirante Padilla, from 2008 to 2010.

From 2010 to 2014, he was with the Department of Electrical Engineering and also with the High-Voltage Research and Test Laboratory (LINEALT), UC3M. He is currently a Professor with the Department of Electrical Engineering, Federico Santa María Technical University, Santiago, Chile. His research interests include partial discharges, insulation systems diagnosis, and instrumentation, and measurement techniques for high frequency currents.

GONZALO AVARIA was born in Concepción, Chile, in 1980. He received the B.Sc. degree in physics from the Universidad de Concepción, Concepción, in 2002, and the Ph.D. degree in physics from the Pontificia Universidad Católica de Chile, Santiago, Chile, in 2008.

From 2009 to 2011, he was a Postdoctoral Fellow with the NSF Engineering Research Center for Extreme Ultraviolet Science and Technology, Colorado State University, Fort Collins, CO, USA. Since 2011, he has been a Researcher with the Departamento de Ciencias Nucleares, Comisión Chilena de Energía Nuclear, Santiago. His current research interests include plasma spectroscopy, dense transient plasmas, pulsed capillary discharges, plasma focus discharges, and transient plasma diagnostics.

Dr. Avaria is a member of the American Physical Society and the Chilean Physical Society. He was a recipient of the Universidad de Concepción Award for Outstanding Student, in 2002.

MARCOS A. DÍAZ received the bachelor's degree in electrical engineering from the University of Chile, in 2001, and the M.S. and Ph.D. degrees in electrical engineering from Boston University, USA, in 2004 and 2009, respectively. He is currently an Assistant Professor with the Department of Electrical Engineering, University of Chile. His research interests include ionospheric turbulent plasma, incoherent scatter radar techniques, low-frequency-radio-astronomy/space instrumentation, and nanosatellite technologies. He is responsible for the Space and Planetary Exploration Laboratory (SPEL), a multidisciplinary Laboratory in the Faculty of Physical and Mathematical Sciences, University of Chile, which hosts the University Nanosatellite-Based Space Program.

CRISTIAN PAVEZ was born in Santiago, Chile, in 1972. He received the B.S. and M.S. degrees in physics from the Pontificia Universidad Católica de Chile, Santiago, in 1998 and 2005, respectively, the Ph.D. degrees from the University of Concepción, Concepción, Chile, in 2007, where he is developing his Ph.D. thesis in experimental plasma physics with the Plasma Physics and Nuclear Fusion Laboratory, Comisión Chilena de Energía Nuclear (CCHEN).

In December 2008, he joined the CCHEN Plasma Group as a Researcher. Since 2016, he has been an Adjunct Associate Researcher of the Ph.D. Program in physics with Physical Sciences Department, Universidad Andres Bello, Chile. His current research interests include dense transient plasmas, including Z-pinch, plasma focus and capillary discharges, transient plasma diagnostics, optical and digital holography, optical and digital interferometry, and optical refractive diagnostics. He is a member of the Optical Society (OSA) and the Chilean Physical Society (SOCHIFI).

ROGER SCHURCH (S'11–M'15) received the degree in electrical engineering from Federico Santa María Technical University (UTFSM), Valparaiso, Chile, in 2006, and the Ph.D. degree from The University of Manchester, in 2014. He was a High Voltage Equipment Analyst with Transelec Transmission Company, before joining UTFSM, as a Lecturer, in 2008. He joined UTFSM as an Assistant Professor. His research interests include electrical trees and partial discharges, and insulation diagnostics of power system plant.

LEOPOLDO SOTO received the B.S., M.S., and Ph.D. degrees in physics from the Pontificia Universidad Católica de Chile, Santiago, in 1989, 1990, and 1993, respectively. He is currently the Head of the Plasma Physics and Nuclear Fusion Laboratory, Comisión Chilena de Energía Nuclear (CCHEN), and the Director of the Center for Research and Applications in plasma physics and pulsed power, P4. He is also an Associate Professor of the Ph.D. Program in physics with the University of Concepción, Chile, and the Ph.D. Program in applied science with the University of Talca, Chile, and an Associate Full Professor with the Physical Sciences Department, Universidad Andres Bello, Chile. His current research interests include dense transient plasmas, pulsed power and applied optics, especially Z-pinch, plasma focus, nuclear fusion mechanisms, capillary discharges, pulsed power miniature devices, effects of pulsed radiation on materials and on biological objects, transient plasma diagnostics, holography, interferometry, and optical refractive diagnostics.

In 2007, he was elected as a Fellow of the Institute of Physics, U.K. In 1999, he was awarded with a Presidential Chair in science by the President of Chile. He was the President of the Chilean Physical Society, SOCHIFI, for two periods, from April 2003 to April 2008, and a Secretary General from April 2017 to April 2019. Since June 2017, he is also a Scientific Advisory of the Commission of Challenges of the Future, Science, Technology and Innovation, Senate of the Republic of Chile.